Australia's Future Extratropical Cyclones

ACACIA S. PEPLER[a] AND ANDREW J. DOWDY[a]

[a] *Bureau of Meteorology, Melbourne, Victoria, Australia*

(Manuscript received 28 April 2022, in final form 18 July 2022)

ABSTRACT: Extratropical cyclones are responsible for the majority of total and extreme rainfall in many regions of the extratropics, including in southern Australia. Using an ensemble of projections from 12 regional climate models, we show that both the number of cyclone days and total cyclone-related rainfall are projected to decline across southern Australia during the twenty-first century. This is a robust signal in projections across models and explains more than 80% of projected declines in total cool-season rainfall in the region. Using cyclone-centered composites, we show that cyclone intensity based on wind speed is projected to decrease but cyclone maximum rainfall is projected to increase by close to 7% K^{-1} in the southeast. This results in a shift in the distribution of cyclone rainfall, with a decrease in moderate rainfall but little change or an increase in extreme rainfall.

SIGNIFICANCE STATEMENT: Extratropical cyclones are very important for southern Australian rainfall, and they are expected to become less frequent in a warming climate. Our research shows this explains at least 80% of the projected decline in cool-season rainfall in southern Australia. However, the frequency of extratropical cyclones with very heavy rainfall may increase, particularly in Tasmania and the southeast coast, with increases in rainfall intensity in line with the Clausius–Clapeyron relationship. This contributes to increases in the frequency of very heavy rainfall in the future.

KEYWORDS: Australia; Cutoff lows; Extratropical cyclones; Rainfall; Climate change; Regional models

1. Introduction

Extratropical cyclones, and their associated fronts, are responsible for the majority of total rainfall in the extratropics and are particularly important for rainfall extremes and flood risk (Dowdy and Catto 2017; Pepler and Dowdy 2021a; Pfahl and Wernli 2012; Utsumi et al. 2017). In a warming climate, the Southern Hemisphere storm track is expected to move poleward, with a corresponding decline in cyclone frequency in the Southern Hemisphere midlatitudes (Utsumi et al. 2016; IPCC 2021). However, the projected changes in cyclone frequency and rainfall can vary significantly depending on the type of cyclone, including between cyclones with different vertical structures. In particular, some areas of the subtropics are projected to experience a decline in the deep, vertically organized cyclones that are most important for rainfall, but a simultaneous increase in shallow surface cyclones, including over land areas in the summer months (Pepler and Dowdy 2021a).

These projections have a range of uncertainties including due to the relatively coarse resolution of global climate models (GCMs), which renders them unable to represent details for smaller-scale surface cyclones as well as processes associated with heavy and extreme rainfall. Notably, GCMs consistently underestimate the frequency of surface cyclones over much of the Southern Hemisphere midlatitudes, including their contribution to total and extreme rainfall (Pepler and Dowdy 2021a). Given the high contribution of cyclones to rainfall in this region, and the magnitude of projected declines, this may translate to an underestimation of the true projected rainfall declines for these highly populated areas including southern Australia, South Africa, and South America. Consequently, improved model projections for cyclone structure would improve decision making for water availability and risks associated with extremes including flooding.

In Australia south of 25°S, surface cyclones are responsible for over 40% of rainfall, and more than 50% of heavy rainfall, particularly during the cooler months and near the southern and eastern coasts (Pepler et al. 2020). Heavy rainfall is particularly likely during deep cyclones where a surface cyclone is vertically well organized to at least 500 hPa (Pepler and Dowdy 2020, 2021b) or when a surface cyclone coincides with thunderstorm activity (Dowdy and Catto 2017; Pepler et al. 2020). To date, detailed projections of future Australian cyclones have focused largely on the east coast (Cavicchia et al. 2020; Dowdy et al. 2014; Pepler et al. 2016a), where cyclones are projected to decrease in frequency but increase in rainfall intensity. However, both observations and model projections indicate that declining cyclone frequency may play an increasingly important role in historical and future rainfall

Denotes content that is immediately available upon publication as open access.

Supplemental information related to this paper is available at the Journals Online website: https://doi.org/10.1175/JCLI-D-22-0312.s1.

Corresponding author: Acacia Pepler, acacia.pepler@bom.gov.au

DOI: 10.1175/JCLI-D-22-0312.1

© 2022 American Meteorological Society. For information regarding reuse of this content and general copyright information, consult the AMS Copyright Policy (www.ametsoc.org/PUBSReuseLicenses).

Unauthenticated | Downloaded 06/19/24 09:21 PM UTC

declines elsewhere in southern Australia including in eastern parts away from the coast (Pepler et al. 2019; Risbey et al. 2013; Utsumi et al. 2016).

Downscaling to finer resolution from GCMs using regional climate models (RCMs) has previously been found to improve on some aspects of projections, both in terms of the representation of cyclones (Di Luca et al. 2016) and the representation of rainfall processes and extremes, particularly in areas such as the coasts and over topography (Di Virgilio et al. 2020). In recent years, several new regional downscaling experiments have become available for Australia based on phase 5 of the Coupled Model Intercomparison Project (CMIP5; Taylor et al. 2012) with three different RCM approaches providing data for downscaled climate change projections throughout Australia (as detailed in section 2). These downscaling data allow a new evaluation of the ability of RCMs to represent cyclones and their rainfall, as well as new insight into how cyclones and their rainfall could change in future projections of Australian climate.

In this paper we evaluate the skill of 12 RCMs to represent cyclone frequency and rainfall over Australia, in comparison with 10 CMIP5 GCMs, with particular attention paid to vertically well-organized ("deep") cyclones. We then assess projected changes in cyclone frequency and associated heavy and extreme rainfall, showing that declines in deep cyclones are the main cause of projected rainfall declines in southern Australia. Last, we use cyclone-centered composites to assess changes in the synoptic characteristics and rainfall intensity of future cyclones in southwestern Western Australia (SWWA), Tasmania (TAS), the eastern seaboard (ESB), and elsewhere in southeast Australia (SEA).

2. Methods

a. *Cyclone tracking*

The University of Melbourne cyclone tracking scheme is used to identify cyclones in this study (Murray and Simmonds 1991; Simmonds et al. 1999). This is one of the most widely used cyclone tracking methods, and it compares well to other approaches in intercomparison studies, including when evaluated against observed cyclone datasets (Neu et al. 2013; Pepler et al. 2015). The code is freely available online (https://cyclonetracker.earthsci.unimelb.edu.au), with additional scripts for pre- and postprocessing data also available (https://github.com/apepler/cyclonetracking/).

In this tracking method, gridded fields are first converted to two hemispheric grids using a polar stereographic projection with an approximate resolution of 1.5° at 30°S, with 2° of spatial smoothing applied. This allows results to be compared fairly between models of varying spatial resolutions while minimizing the detection of small-scale lows, which can vary substantially between observed datasets (Di Luca et al. 2014). Cyclones are identified as local maxima in the Laplacian of the gridded field, which are then linked with a nearby field minimum, with both open and closed depressions included to allow for the coarser spatial resolution of CMIP5 models. Cyclones are then joined into tracks using a probability matching technique. Surface cyclones are not tracked where model orography is above 1000 m, noting that the orography varies between models of different resolutions.

Cyclones are tracked using both 6-hourly mean sea level pressure (MSLP) and daily mean 500-hPa geopotential height. The coarser temporal resolution for upper lows was necessitated by the data resolution of CMIP5 but was also found to better identify the slow-moving upper lows that are most likely to be associated with heavy rainfall (Pepler and Dowdy 2021b). The average Laplacian of MSLP (or geopotential height) within a 2° radius of the cyclone center is related to the cyclone's vorticity, and is used as the primary measure of cyclone intensity. After matching reanalysis-based cyclones with an observed dataset of cyclone frequency in east Australia (Pepler and Dowdy 2021b), minimum intensity thresholds of 0.8 hPa $(^\circ \text{ lat})^{-2}$ for surface lows and 6 m $(^\circ \text{ lat})^{-2}$ at 500 hPa were applied to all datasets to remove some of the very weak and small-scale cyclones that high-resolution datasets generate, which are not relevant to rainfall impacts (Di Luca et al. 2014). This method has been applied to cyclones across Australia and can identify many low pressure systems in tropical areas, but it may not capture all tropical cyclones, particularly those with small spatial scales. Consequently, our study focuses on the regions south of 25°S that are dominated by larger extratropical and subtropical cyclones and have more robust projected changes.

In this paper we distinguish between "deep" cyclones, which extend through much of the troposphere and can be identified both near the surface as well as at 500 hPa, and "shallow" cyclones, which occur over a restricted range of levels and therefore can be identified only at the surface or at 500 hPa (but not both). We use the simplified method of Pepler and Dowdy (2021a), which requires only 6-hourly surface cyclones identified using MSLP, as well as upper cyclones identified on the 500-hPa geopotential height, with cyclones considered to be deep if they can be simultaneously identified at both layers within a 500-km radius. First, an individual surface cyclone was classified as deep if there was a corresponding low at 500 hPa on the same UTC day within a 5° radius, and the same process was used to identify deep 500-hPa cyclones with a corresponding surface low. Second, a cyclone track was classified as deep if it was deep at any time during the track, to allow for the temporal development of cyclones that are most well organized subsequent to the period of heaviest rainfall (Booth et al. 2018; Pepler and Dowdy 2020). The remaining tracks at each level are classified as shallow.

Daily grids of cyclone occurrence were generated by expanding the locations of all cyclones on a given day such that they influence a circle with 10° radius, centered on the cyclone center, consistent with the observed radius of cyclone-associated rainfall (Hawcroft et al. 2012; Booth et al. 2018; Utsumi et al. 2017). A point was classified as influenced by a deep cyclone on a given day if it was influenced by a deep cyclone at either the surface or upper level; as a shallow surface cyclone if it was influenced by a shallow surface cyclone but no deep cyclone; and as a shallow upper cyclone if there was a shallow upper cyclone but no deep or shallow surface system.

Unauthenticated | Downloaded 06/19/24 09:21 PM UTC

TABLE 1. RCM ensembles (rows) and corresponding CMIP5 models (columns).

	ACCESS1.0	ACCESS1.3	CanESM2	GFDL-ESM2M	MIROC5	NorESM1-M
BARPA	X					
NARCliM (×2)	X	X	X			
CCAM	X		X	X	X	X

b. Datasets

Cyclone tracking was first applied to three high-resolution modern reanalyses, to allow for observational uncertainty in assessing model biases: ERA5 (Hersbach et al. 2020), JRA-55 (Kobayashi et al. 2015), and the Bureau of Meteorology Atmospheric High-Resolution Regional Reanalysis for Australia (BARRA; Su et al. 2019). Cyclone tracks for 10 CMIP5 global climate models were also obtained from Pepler and Dowdy (2021a), which are available online (https://doi.org/10.6084/m9.figshare.13393172). In addition, cyclone tracking was performed on three regional downscaling ensembles, downscaling CMIP5 data over the Australian region (Table 1; Dowdy et al. 2021).

The New South Wales and Australian Capital Territory Regional Climate Modeling (NARCliM1.5; Evans et al. 2021) incorporates three CMIP5 models downscaled using two different versions of the Weather Research and Forecasting (WRF) Model for the CORDEX-Australasia region on a rotated grid, which was bilinearly regridded to a regular 0.5° grid prior to analysis. In addition, five CMIP5 models were downscaled using the Conformal Cubic Atmospheric Model (CCAM) for the Australian region, with data available on a 0.12° grid (Thatcher and McGregor 2011). One CMIP5 model (ACCESS1.0) was downscaled to 0.12° using the Bureau of Meteorology Atmospheric Regional Projections for Australia (BARPA; Su et al. 2021) modeling approach. BARPA downscaled the eastern and western halves of Australia separately (due to the priorities of various previous projects for their areas of interest), with those BARPA data later joined at 128.5°E to help provide national coverage, noting some anomalies near the model boundary that may be relevant when interpreting results in that central region.

All of these three RCMs (NARCliM1.5, CCAM, and BARPA) have data available for the historical period 1980–2005 and both a medium (RCP4.5) and high (RCP8.5) emission pathway for 2006–99. The model domains for each RCM are shown in Fig. 1, with cyclone tracking for each model performed for a region 5° from the model boundary, to minimize boundary effects; this results in slightly different domains for each RCM, although all have cyclone data available over the entire Australian region (Fig. 1). ERA5 and CMIP5 cyclones were tracked over the entire globe. Results will focus on the region common to all RCMs: 110°–160°E, 10°–45°S.

Cyclone-centered composites of 6-hourly instantaneous 10-m wind, MSLP, and 500-hPa geopotential height were extracted for ERA5 and the 12 RCMs for a 10° region surrounding the cyclone center for both the historical and RCP8.5 simulations. All precipitation observations within ±3 h of the cyclone observation were extracted and then averaged to calculate the rain rate for each cyclone, using the highest frequency data available. This was extracted on the 0.5° grid for NARCliM and 0.25° for ERA5, but downgraded to 0.24° for CCAM and BARPA, for ease of comparison. For each cyclone, we also calculated a range of statistics including the highest rain rate and wind speed within 10° of the cyclone center and the average rain rate within 5° of the cyclone center, noting that this average is calculated across both the areas of high cyclone rainfall to the south and east of the cyclone center and areas with little rainfall to the northwest.

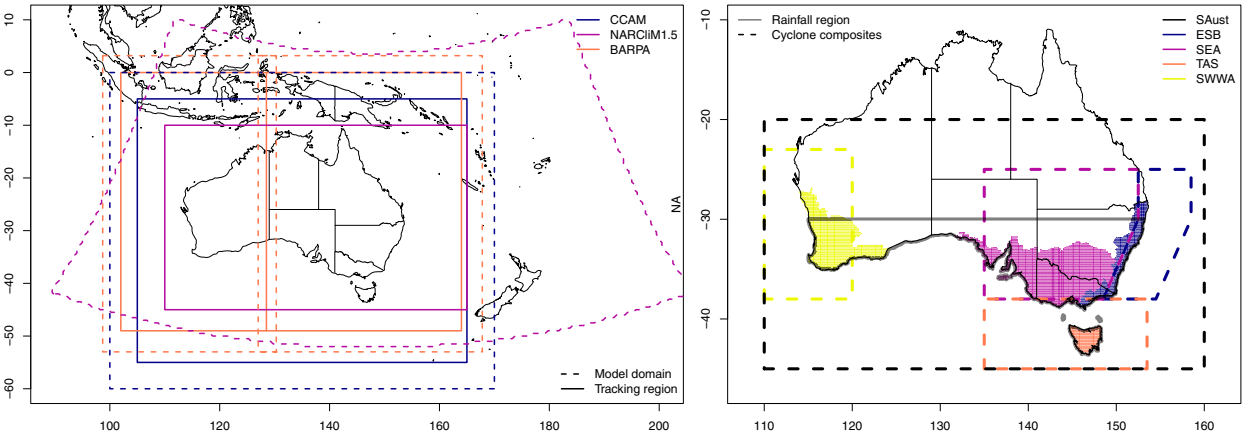

FIG. 1. (left) Dashed outlines show the domain for each RCM ensemble, with the two BARPA regions overlapping. Solid outlines show the regions used for cyclone tracking, noting the boundary at 128.5°E where the BARPA simulations are combined. (right) Shading indicates the four subregions of southern Australia, with dashed outlines indicating the corresponding domains used for cyclone composites.

Unauthenticated | Downloaded 06/19/24 09:21 PM UTC

Composites are calculated over all detected cyclones, so can include many time steps from a single event; this increases the sample size and ensures that all cyclones of interest are considered, particularly as cyclones may reach their highest intensities once they have moved over the Tasman Sea and away from the land. However, sensitivity tests showed that projected changes in cyclone-centered rainfall are similar when only the time of heaviest rainfall is considered (not shown). No rotation is applied to the composite data, such that the composite means resemble the observed cyclone structure for each region of Australia.

The contributions of reanalysis cyclones to total and extreme rainfall over Australia were identified by matching the grids of daily cyclone occurrence to a daily 0.05° gridded analysis of observed rainfall based on station data, which is the most widely used and reliable rainfall dataset for Australia that was available for use in this study [Australian Gridded Climate Data (AGCD); Jones et al. 2009]. The contribution of cyclones was also calculated for four intensity thresholds: 1 mm, 10 mm, and local heavy rainfall thresholds corresponding to the 99th and 99.7th percentiles calculated from AGCD (calculated for the 30-yr period 1976–2005). For comparison, rainfall from RCM cyclones was calculated using rainfall that had been regridded to the same spatial grid over Australia, and bias corrected using the quantile matching for extremes method (Dowdy 2020b), allowing the same percentile thresholds to be applied to model rainfall.

For the purposes of this study, the historical period is referred to as the 30-yr period 1980–2009, which includes 2006–09 data obtained from the RCP8.5 simulation, noting that the end of this period in 2009 is already more than 10 years in the past. Of the set of modeled greenhouse gas emission pathways provided in CMIP5, observed climate change trends for temperature indicate that this high emissions pathway RCP8.5 has been followed more closely than low emissions pathways (Schwalm et al. 2020). To maximize signal-to-noise ratios, projections are taken as the difference between 2070–99 and 1980–2009 using data for the high emissions pathway (RCP8.5). This is then divided by the change in global mean temperature, which was calculated for the corresponding GCM over the same period, such that trends are reported as a magnitude per degree of global warming, an approach that allows potential changes to be compared without the added uncertainty related to future greenhouse gas emissions pathways or a GCM's climate sensitivity (Pendergrass et al. 2015). We used the NARCliM ensemble to test the sensitivity of our results to the choice of emissions pathway and found that projected changes per degree of warming were very consistent between RCP4.5 and RCP8.5, with slightly larger changes per degree in the RCP4.5 ensemble. For the purposes of this study, the cool season is defined as May–October and warm as November–April.

In addition to spatial plots, we investigated detailed changes in cyclones and rainfall for southern Australia (land areas south of 30°S) as well as five subregions (Fig. 1b), based on a widely used regional classification approach for Australia (CSIRO and BoM 2015). These regions were defined by combining subregions [from CSIRO and BoM (2015)] into broader regions that better match the regions identified as experiencing similar weather by Fiddes et al. (2021).

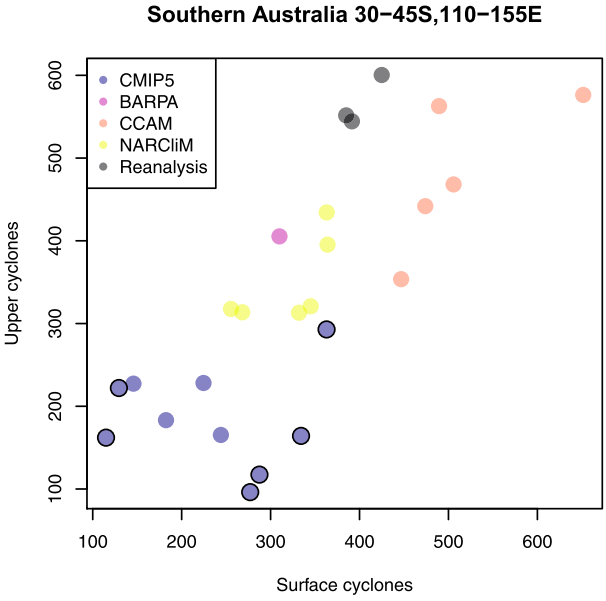

FIG. 2. Annual number of surface and upper cyclone observations in Southern Australia (30°–45°S, 110°–155°S) during 1980–2009 for 3 reanalyses, 10 CMIP5 models, and 12 RCMs. Black rings indicate the CMIP5 models used for downscaling. Because surface cyclones are identified every 6 h, upper cyclone counts are multiplied by 4 for comparison.

The subregions of SWWA and SEA have both seen significant cool-season rainfall decline in recent years, with future declines projected in climate model simulations (BoM and CSIRO 2020). The ESB is an area where cyclones are particularly important for both water security and coastal flooding, so an area where future changes in cyclones is of keen interest (Callaghan and Power 2014; Pepler and Rakich 2010). TAS, to the south of mainland Australia, is an important hydropower region where cool-season rainfall is projected to increase. Four corresponding regions were also selected for extracting cyclone composites, based on the preferred location of cyclones on days with widespread heavy rainfall in each region following the approach used to identify the location of cyclones that produced heavy east coast rain in Pepler and Dowdy (2021b).

3. Model evaluation

Figure 2 shows the annual number of cyclones identified across southern Australia during the common period 1980–2009. CMIP5 models produce about 60% as many surface lows as the reanalysis datasets, and 33% of the observed number of upper lows. This negative bias led to Pepler and Dowdy (2021a) employing model-dependent thresholds of minimum cyclone intensity so as to retain similar cyclone counts in all GCMs to a reanalysis-based climatology. In comparison with GCMs, the mean frequency of surface cyclones in RCMs is close to reanalyses, with CCAM tending to overestimate and NARCliM and

Unauthenticated | Downloaded 06/19/24 09:21 PM UTC

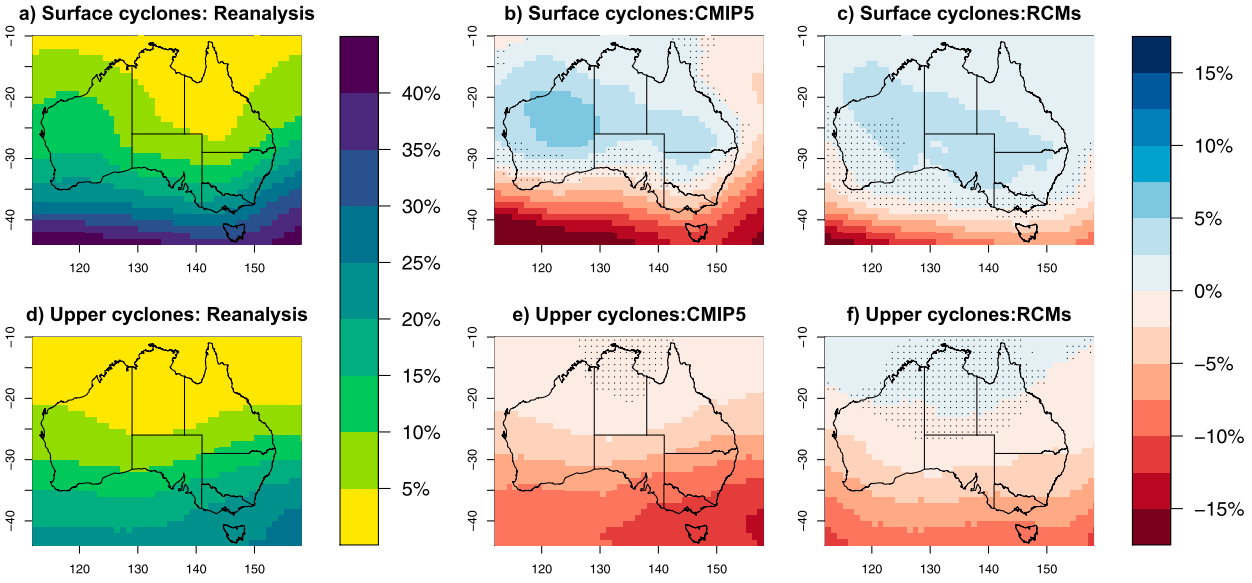

FIG. 3. The average percentage of days per year with a (a) surface or (d) upper cyclone center located within a 10° radius, averaged across the ERA5 and JRA-55 reanalyses, for 1980–2009. (b),(e) The respective differences between the average cyclone frequency in CMIP5, over 1980–2009, and (a) and (d), with stippling indicating where this is smaller than the difference between the two reanalyses. (c),(f) As in (b) and (e), respectively, but for the 12 RCMs.

BARPA tending to underestimate numbers when compared with observed frequencies. The frequency of upper lows continues to be underestimated in RCMs, particularly in NARCliM, but to a lesser extent than in the driving GCMs.

Figures 3a and 3d show the average number of days per year (in percent) influenced by a cyclone, defined as days with a cyclone center within a 10° radius, averaged across the two reanalysis datasets. Surface cyclones are common to the south of Australia and in the Tasman Sea to the southeast, with an area of high frequency also identified in parts of Western Australia; this is due to the sensitivity of this tracking method to the west Australian coastal trough. While surface cyclones occur preferentially over water, upper cyclones are more uniformly observed south of ~30°S. The CMIP5 models underestimate the frequency of upper cyclones everywhere and surface cyclones in the areas of peak frequency so the south and east of Australia, while overestimating surface cyclones over land areas. Biases in the frequency of upper cyclones are present throughout the year but the increased frequency of surface cyclones over areas is a warm-season phenomenon, when CMIP5 models generate too many cyclone centers over the west and east coasts (not shown). In contrast, the CMIP5 models underestimate surface cyclone frequency south of 35°S during the cool season when cyclones make their largest contribution to rainfall.

The spatial pattern of biases in RCMs is consistent with that in GCMs but the overall frequency of cyclones is higher, consistent with Fig. 2, which acts to reduce the biases over southern Australia, particularly during the cool season. For upper cyclones in particular, the majority of RCMs have smaller biases than the GCM mean across most of southern Australia (Fig. S1 in the online supplemental material), which is also true for surface cyclones in the Tasman Sea. In other areas, some RCMs improve on the GCM ensemble mean, while others have larger biases. Inspection of individual RCMs (Figs. S2 and S3 in the online supplemental material) shows that the frequency of upper cyclones over Australia is most consistent with the reanalyses in CCAM, but these RCMs tend to overestimate surface cyclone frequency across Australia and the surrounding oceans. In comparison, BARPA and NARCliM tend to underestimate the frequency of both upper and surface cyclones to the south of Australia but have smaller biases in surface cyclones over land areas. The larger biases south of 40°S are likely associated with the smaller poleward extent of the analysis region for these RCMs (Fig. 1a), resulting in difficulties in detecting cyclone centers at these latitudes.

Consistent with the lower counts of upper cyclones in the RCMs, the RCMs tend to underestimate the frequency of deep cyclones and overestimate the frequency of shallow surface cyclones when compared with the ERA5 reanalysis (Table 2). Consequently, while the proportion of rainfall due to cyclones is similar between both ERA5 (52%) and the RCMs (49%), the RCMs underestimate the contribution arising from deep and shallow upper cyclones. Deep cyclones have heavier average rain rates than shallow surface cyclones and are particularly important for heavy rainfall above the 99.7th percentile, explaining 52% of such events in ERA5 and 40% in the RCMs. Deep cyclones are more common in the cool season, where they are responsible for 44% of total rainfall and 66% of days above the 99.7th percentile in ERA5, while shallow surface cyclones are more common in the warm season. The RCMs replicate this seasonal variation in cyclone frequency.

Unauthenticated | Downloaded 06/19/24 09:21 PM UTC

TABLE 2. Average rainfall and days above various intensity thresholds for southern Australia (land areas south of 30°S) in AGCD, the proportion that occur on days with a deep cyclone, a shallow surface cyclone, or a shallow upper cyclone in ERA5, and the RCM ensemble mean proportion from each cyclone type.

		Percent from cyclones in ERA5			Percent from cyclones in RCMs		
	Mean	Deep	Surface	Upper	Deep	Surface	Upper
Total rain	466.2 mm	40%	6%	6%	30%	14%	4%
Days per year	—	15%	5%	4%	11%	8%	3%
Days ≥ 1 mm	66.7	33%	5%	6%	25%	13%	4%
Days ≥ 10 mm	12.6	45%	7%	6%	33%	16%	4%
Days ≥ Q99	3.7	48%	8%	6%	36%	17%	4%
Days ≥ Q99.7	1.0	52%	9%	6%	40%	18%	4%

Spatially, deep cyclones are most important for rainfall in southern Australia, particularly in Tasmania and the southeast where they explain over 50% of annual rainfall (Fig. 4). Deep cyclone rainfall in this region is consistently underestimated by the RCMs, but particularly in SWWA and Tasmania and in the NARCliM simulations (Fig. S4 in the online supplemental material). This is in part due to the proximity of these regions to the boundaries used for cyclone tracking in NARCliM, meaning that the tracking may miss some of the cyclones influencing these regions. This is particularly important because, in contrast to the east coast, deep cyclones that influence southeastern Australia frequently have the upper low situated to the south of the surface low (Pepler and Dowdy 2021b). While shallow surface lows are most important to rainfall over inland areas in ERA5, these are increasingly important for southern regions in the RCMs (Fig. S5 in the online supplemental material), suggesting that some of these may have been considered deep lows if not for model biases in upper cyclones.

Figure 5 shows the average ERA5 rain rate, wind speed, and mean sea level pressure composites for deep and shallow cyclones in the five regions from Fig. 1b. Deep cyclones (Figs. 5f–j) have consistently deeper MSLP centers and stronger wind speeds than shallow cyclones and have higher average rain rates within 5° of the cyclone center. However, there is significant variability between cyclones in different parts of Australia. In SWWA, shallow cyclones are typically very small lows identified in a coastal trough and have very low rain rates, while the average SEA shallow low is also embedded in a trough with low rainfall and weak wind speeds. Many of the shallow surface lows identified in these regions may thus be the western Australian coastal trough (Fandry and Leslie 1984) or heat lows (Lavender 2017). In comparison, shallow cyclones in Tasmania have different spatial structures to deep cyclones, but similar average wind speeds and rain

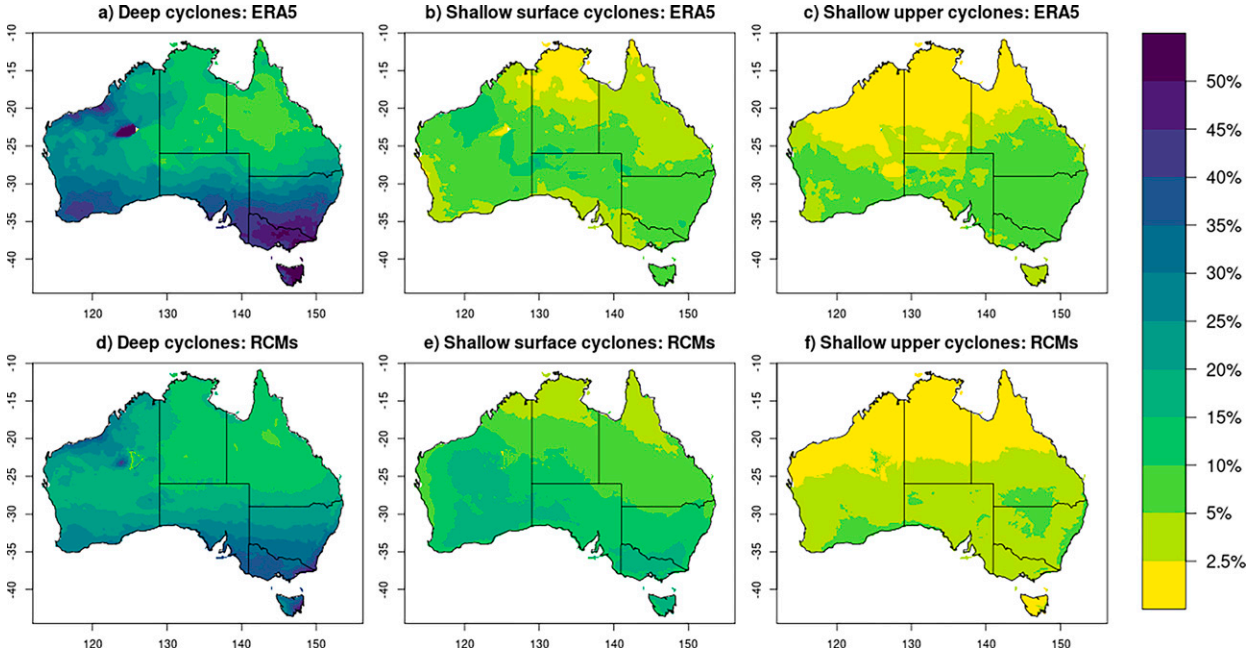

FIG. 4. The contribution (%) of three cyclone categories to annual rainfall, over 1980–2009, from (a)–(c) ERA5 and (d)–(f) the RCM ensemble mean.

Unauthenticated | Downloaded 06/19/24 09:21 PM UTC

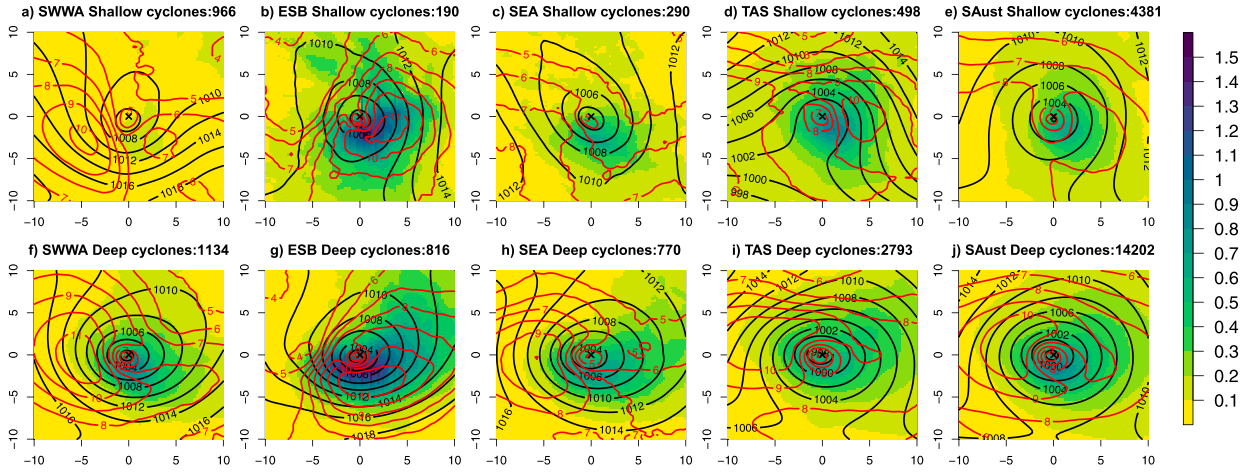

FIG. 5. Composite 6-h mean rain rate (shaded; mm h^{-1}), instantaneous wind speed (red contours; every 1 m s^{-1}), and mean sea level pressure (black contours; every 2 hPa) within ±10° of the cyclone center for all cyclones identified in ERA5 between 1980 and 2009, for (a)–(e) shallow surface cyclones and (f)–(j) deep cyclones. Columns show cyclones in five different subregions, with all southern Australian cyclones in (e) and (j).

rates, as shallow cyclones in this region are less likely to be heat lows and are more likely to embedded in prevailing westerly flow.

Cyclones identified in the ESB are typically stronger and more impactful than elsewhere in southeast Australia, with average rain rates for deep cyclones twice that of any other region. While shallow cyclones in this region are weaker than deep cyclones, their mean rain rates exceed those for deep cyclones elsewhere in Australia. The spatial structure of these cyclones also differs from other regions, with strongest winds and rainfall to the south of the cyclone center for deep cyclones, and shifting southeast for shallow cyclones. These differences in structure are likely related to the interaction of cyclones with high pressure systems, enhancing winds to the south of the cyclone, as well as enhanced rainfall where onshore winds interact with coastal topography (Hopkins and Holland 1997). The large variations in cyclone structure and intensity necessitate the use of several subregions for considering cyclone composites.

Figure 6 shows the same fields as Fig. 5, but averaged across all 12 RCMs. The ensemble mean cyclone structure is very consistent with the fields shown in Fig. 5, showing the RCMs can simulate the different characteristics of cyclones in different parts of Australia. Biases in cyclone-centered rainfall rates are small (Fig. S6 in the online supplemental material), and average to less than 2% across all southern Australian cyclones; shallow cyclone rainfall is slightly overestimated in SWWA (+10%) and ESB (+7%) and underestimated in SEA (−14%) and Tasmania (−13%), while deep cyclone rainfall is underestimated in SWWA (−13%) and overestimated in SEA (+8%). Individual models can have larger biases, particularly shallow cyclones in SEA and SWWA where the historical average rain rates are low (not shown). Average wind speeds are slightly stronger in the RCMs than in ERA5, with biases in mean wind speeds within 5° of the center for individual models and regions of between −0.7 and +1.9 m s^{-1}.

4. Projections of cyclones and associated rainfall

Both surface and 500-hPa cyclones are projected to decline in frequency over southern Australia during the twenty-first century (Fig. 7). Although the total historical frequency of cyclones differed between the GCMs and RCMs (Fig. 2), when trends are presented as a percentage change per degree of global warming, they are broadly consistent between the GCM and RCM ensembles. When compared with the host GCMs, the NARCliM and BARPA RCMs tend to produce slightly stronger declines in upper cyclones and similar changes in surface cyclones, while the CCAM RCMs tend to produce slightly stronger declines in surface cyclones in general, with a notable large decline in both surface and 500-hPa cyclones projected for the RCM CCAM-NorESM1-M. As the RCM changes are broadly consistent with those of the GCMs, we will focus on projections from RCMs due to their enhanced resolution of key orographic features and physical processes that can help contribute to more realistic simulations (such as for regional rainfall).

Noting the projected declines in both surface and upper lows, the frequency of deep cyclones is also projected to decrease over southern Australia during the twenty-first century. For every degree of global warming, southern Australia is projected to experience 4.4 fewer days with a deep cyclone (−11% K^{-1}), and 1.1 fewer days with a shallow upper cyclone (−9% K^{-1}). These percentage changes are broadly similar in both seasons, although absolute changes are largest during the cool season when deep cyclones are more common (Fig. 8b). All RCMs project declines in deep cyclone frequency across both seasons, and declines are statistically significant in all cases except for the warm season in CCAM-GFDL-ESM2M.

Unauthenticated | Downloaded 06/19/24 09:21 PM UTC

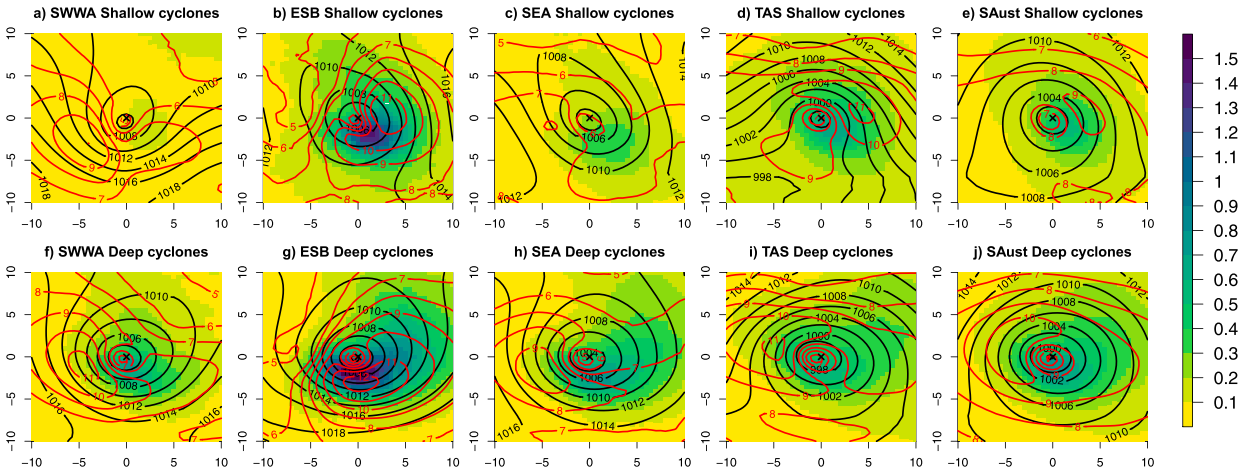

FIG. 6. As in Fig. 5, but averaged across 12 RCMs.

Projected declines are largest in magnitude over southeast Australia and the eastern seaboard during the cool season, including in the Tasman Sea east of Australia.

Little change is projected in the frequency of shallow surface cyclones during the cool season, but for every degree of warming southern Australia is projected to experience 1.8 additional shallow surface cyclone days during the warm season (+9% K^{-1}; Fig. 8g). All RCMs project an increase in the frequency of shallow cyclones during the warm season, and this is statistically significant in all but one case. The projected increase in shallow cyclones is evident across all Australian land areas and the adjacent coastlines but is largest in Western Australia (Fig. 8g), noting that this is a region with a relatively large number of shallow cyclones in the current climate but that they typically produce little rain (Fig. 5).

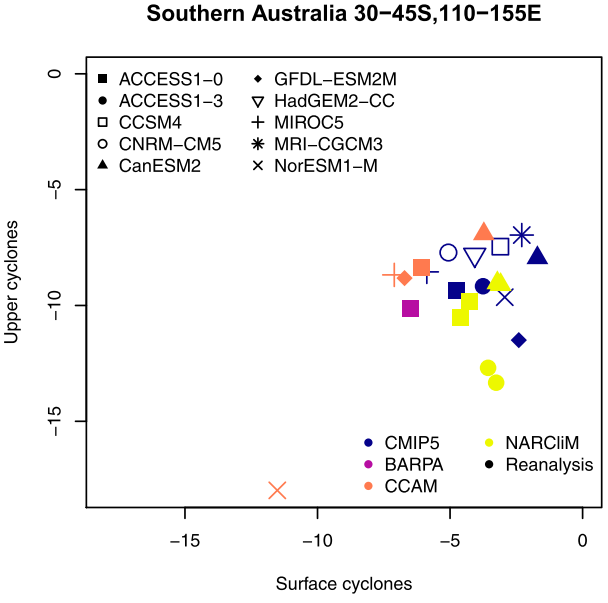

FIG. 7. Projected change in the annual frequency of cyclone centers over southern Australia (110°–155°E, 30°–45°S) between 1980–2009 and 2070–99, in percent per degree of warming, Different symbols indicate the source model, with blue showing CMIP5 projections and other colors showing the different RCMs.

The projected decline in the frequency of deep cyclones in southern Australia has a significant impact on future mean rainfall. During the cool season, when cyclones cause a large proportion of rainfall in southern Australia, total seasonal rainfall is projected to decline by 10 mm for every degree of global warming (−4% K^{-1}), resulting in an overall decline from 255.8 to 220.9 mm by 2070–99 under RCP8.5 (Fig. 8m). More than 80% of this projected decline is due to declining rainfall from deep cyclones (Fig. 8j), which is projected to decrease by 8.8 mm K^{-1} (−10% K^{-1}). All RCMs project a decline in rainfall from deep cyclones in southern Australia, which is statistically significant in all but one case, with particularly large declines projected along the southern and eastern coastlines. In contrast, there is no change projected in rainfall from days without cyclones when averaged across southern Australia, with model agreement on the sign of the change only evident for a decline in no-cyclone rain in parts of SWWA and northeast Australia, and an increase on parts of the mainland east coast and the west coast of Tasmania.

Deep cyclone rainfall is also projected to decline across southern Australia during the warm season (Fig. 8o), by 3.7 mm K^{-1} (−6% K^{-1}), while shallow cyclone rainfall is projected to increase by 2.3 mm K^{-1} (+6% K^{-1}), with these trends consistent across at least 10 out of 12 RCMs (Fig. 8p). This means there is no projected change in total cyclone-related rainfall, but an increasing proportion of warm-season rainfall will be associated with shallow surface cyclones. In contrast to relatively robust results for cyclone-related rainfall, there are large uncertainties between models in projected changes in noncyclone rainfall, with these uncertainties dominating overall projections during the warm season. The much larger uncertainty in projected changes in noncyclone rainfall when compared with the robust declines in deep cyclone rainfall is also evident for each region of southern Australia in Fig. 9a.

Unauthenticated | Downloaded 06/19/24 09:21 PM UTC

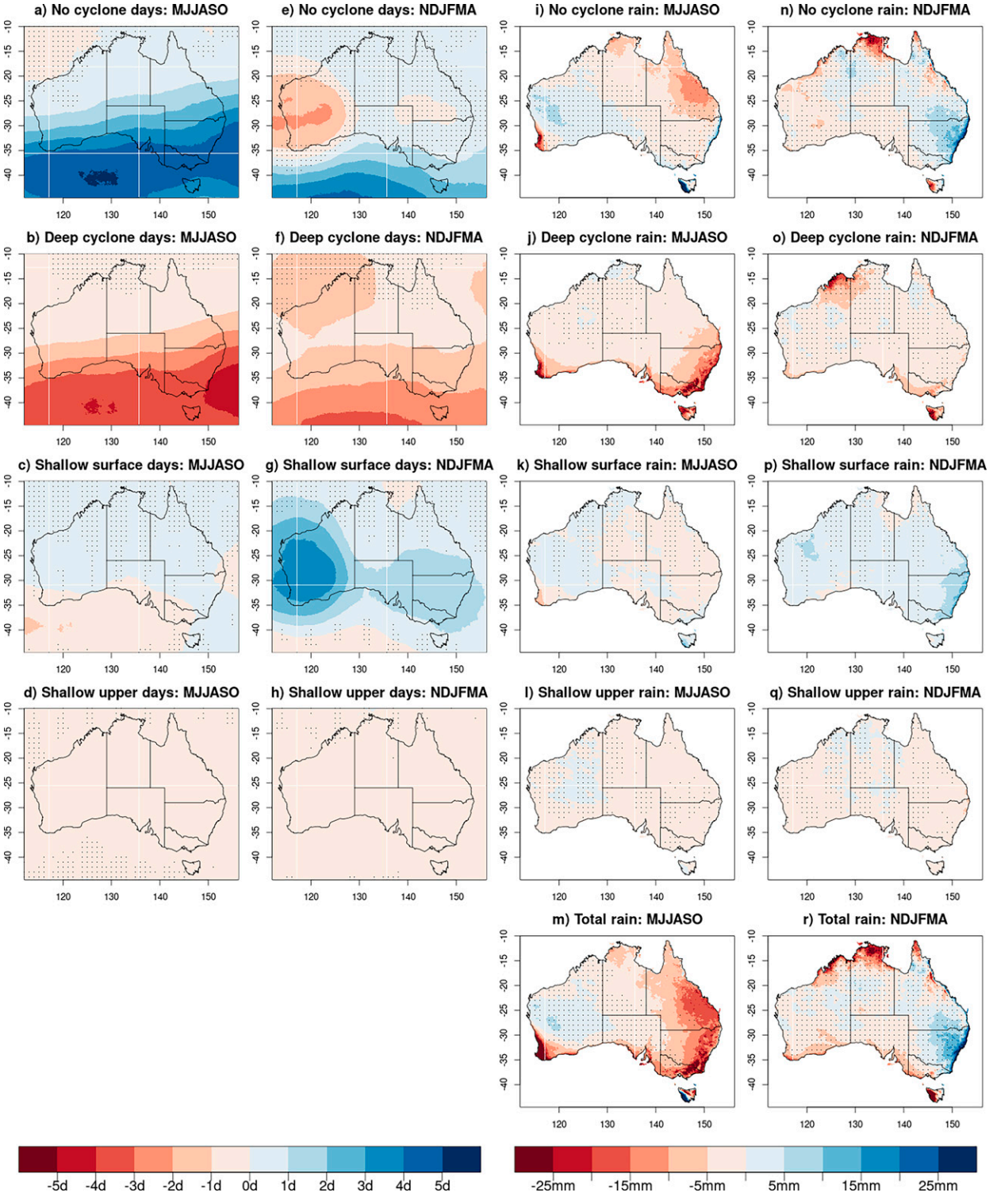

FIG. 8. Change in the mean seasonal number of days per degree of global warming with no cyclone or one of the three cyclone categories between 1980–2009 and 2070–99 from RCP8.5 for the (a)–(d) cool season and (e)–(h) warm season. (right) Also shown is the change in total seasonal rainfall (mm K^{-1}) from days with no cyclone or one of the three cyclone categories between 1980–2009 and 2070–99 from RCP8.5 for the (i)–(l) cool season and (n)–(q) warm season and (m),(r) change in total rainfall accumulated across all categories for the respective seasons. Shading shows the average change across the 12 RCMs; stippling indicates where fewer than 10 models agree on the sign of the change.

Unauthenticated | Downloaded 06/19/24 09:21 PM UTC

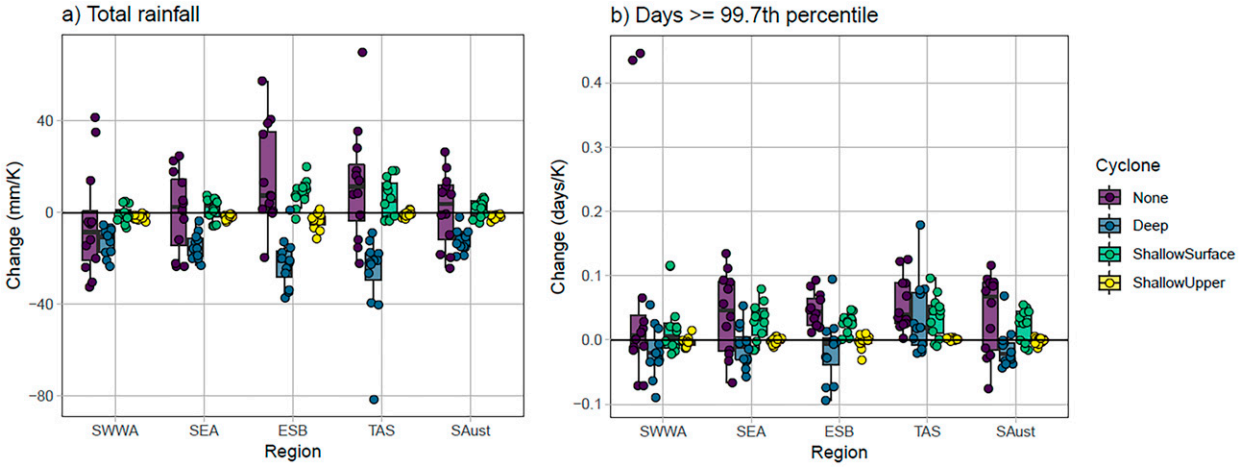

FIG. 9. (a) Projected change in annual rainfall and (b) number of days with daily rainfall totals exceeding the current 99.7th percentile for southern Australia and four subregions (region boundaries indicated in Fig. 2). Each dot gives the change for a single RCM, with colors indicating rainfall change arising from no cyclone days or the three categories of cyclone, as labeled.

Averaged across southern Australia, the annual number of heavy rain days above the 99.7th percentile is projected to increase by 0.05 days K^{-1} (+4% K^{-1}) (Fig. S7 in the online supplemental material), with increases projected in 67% of models (Fig. 9b). Increases are projected across most of eastern Australia, with more than 90% of models projecting an overall increase in heavy rain days in the ESB (+5% K^{-1}) and Tasmania (+12% K^{-1}). In these regions, more than 80% of RCMs project increases in the frequency of heavy rainfall on days with no cyclones as well as on days with shallow surface cyclones, some of which could potentially relate to increased rainfall intensity from convective systems such as thunderstorms (Dowdy 2020a; Pepler et al. 2021). Despite the large and robust decreases in total rainfall from deep cyclones projected for these regions (Fig. 9a), heavy rain days from deep cyclones are projected to increase on average in Tasmania (+6% K^{-1}), with little change projected for the ESB (−2% K^{-1}).

In contrast, there are large uncertainties in projected changes in heavy rain days for SWWA and SEA (Fig. 9b). While there is an overall decrease projected for heavy rain days associated with deep cyclones, this projected decline is weak and not robust between RCMs. In contrast, there is very large uncertainty in future heavy rainfall from noncyclone days in these regions, ranging from a decline in some models to increases of more than 30% K^{-1} in others, with particularly large projected increases in NARCliM-CanESM2.

5. Cyclone-centered composites

The contrast between the projected large declines in cyclone-related rainfall in Figs. 8 and 9a, and the small changes or increases in cyclone-related heavy rain days in Fig. 9b, raises the question of whether the average intensity of cyclones is projected to increase even as their frequency decreases. However, when averaged across all cyclones in southern Australia, more than 90% of models project the average cyclone to become weaker, with an average 0.49 hPa K^{-1} increase in central pressure, 0.017 hPa (deg. lat)$^{-2}$ K^{-1} decrease in the average Laplacian of pressure, and 0.16 m $s^{-1}K^{-1}$ decrease in the mean wind speeds within 5° of the cyclone center (Fig. 10). This is a consequence of both a decrease in the intensity and an increase in the relative frequency of shallow cyclones, particularly in SEA and SWWA, as there are no strong changes in any intensity metric for deep cyclones, which are projected to have consistent decreases in frequency across most of the intensity distribution (Fig. S8 in the online supplemental material).

The average rain rate within 5° of the cyclone center is also projected to decline for shallow cyclones in SEA and SWWA in more than 90% of models, with strongest declines to the west of the cyclone center (Fig. 11). In these regions, the projected increase in the frequency of shallow cyclones is dominated by an increase in the frequency of shallow cyclones with relatively low rain rates (Fig. 12), including a large increase in the number of shallow cyclones that produce little to no rain (below the 5th percentile of current cyclones) indicative of a possible increase in heat lows.

In comparison, deep cyclone rain rates are projected to increase in the ESB and Tasmania in more than 80% of models, with average projected increases of 3.9% K^{-1} and 6.6% K^{-1} respectively for mean rainfall within 5° of the cyclone center (Fig. 11). In addition, all RCMs agree that the average maximum rain rate for deep cyclones is likely to increase, by 7.6% K^{-1} in the ESB and 8.2% K^{-1} in Tasmania, with more than 90% also projecting maximum rain rates to increase for deep cyclones in SEA (+5.2% K^{-1}). Projected increases are most robust to the south of the cyclone center, where the heaviest rainfall occurs in observed cyclones (Fig. 5) and easterly winds advect moisture from the warm Tasman Sea over land areas. While there is more uncertainty in projected changes in mean rainfall for shallow cyclones, there is also a robust increase projected in the average maximum rain rate for shallow cyclones of +5.2% K^{-1} in the ESB and +7.2% K^{-1} in Tasmania.

Unauthenticated | Downloaded 06/19/24 09:21 PM UTC

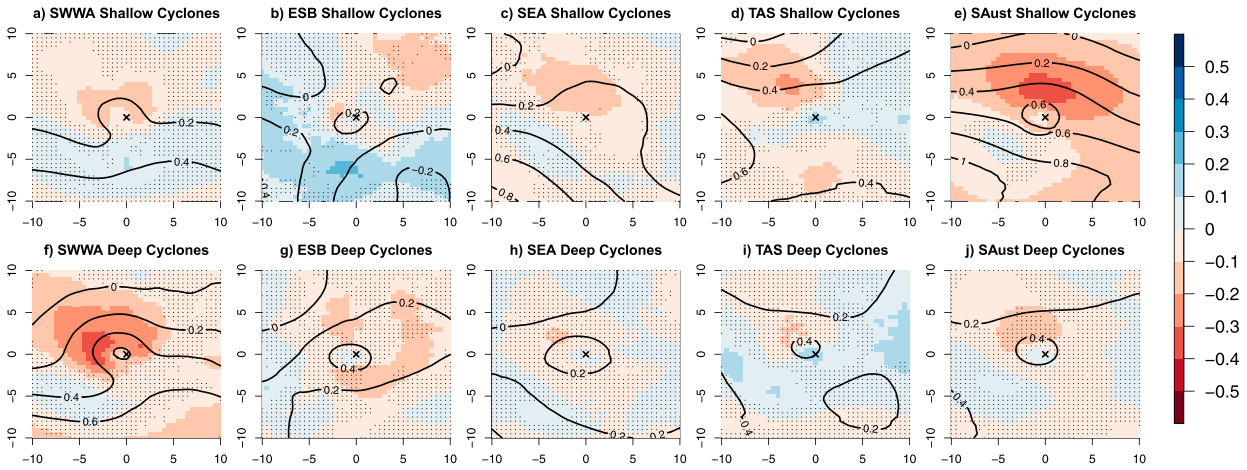

FIG. 10. Ensemble mean change between 1980–2009 and 2070–99 in cyclone-centered wind speeds (shaded; m s^{-1} K^{-1}) and mean sea level pressure (contours; every 0.2 hPa K^{-1}) within ±10° of the cyclone center, for (a)–(e) shallow surface cyclones and (f)–(j) deep cyclones. Columns show cyclones in five different subregions, with all southern Australian cyclones in (e) and (j). Stippling indicates where fewer than 10 models agree on the sign of the change.

The projected increases in mean rain rate and decreases in frequency of deep cyclones in Tasmania and the ESB reflect a change in the distribution of cyclone rainfall (Fig. 12). In these regions, there are large projected declines in the frequency of deep cyclones with low to moderate rainfall, below the 70th percentile of historical cyclones. In contrast, the numbers of both deep and shallow cyclones with mean rain rates above the 95th percentile of historical cyclones are projected to increase in the majority of RCMs, so that in the ESB there are 0.3 additional cyclones per year with mean rainfall above the current 95th percentile for every degree of global warming (+15% K^{-1}), and in Tasmania there is 1.1 additional cyclone per year (+20% K^{-1}). These cyclones have average 6-hourly rain rates exceeding 1.6 mm h^{-1} in the ESB and 1.0 mm h^{-1} in Tasmania when calculated over ERA5, noting that it is a spatial average that includes areas of both low rainfall and areas where rain rates are much higher than the spatial mean (Fig. 5).

The current 95th percentile of maximum rain rate is significantly higher in ERA5, 14.7 mm h^{-1} in the ESB and 6.8 mm h^{-1} in Tasmania. This varies more substantially with model resolution, with NARCliM producing similar or slightly lower values to ERA5 but maximum rain rates at least 50% higher in the higher-resolution CCAM and BARPA simulations. The number of cyclones exceeding the current 95th percentile for maximum rain rate is expected to increase by more than 25% K^{-1} in both regions, such that under RCP8.5 in 2070–99 both the ESB and Tasmania have twice as many cyclones with

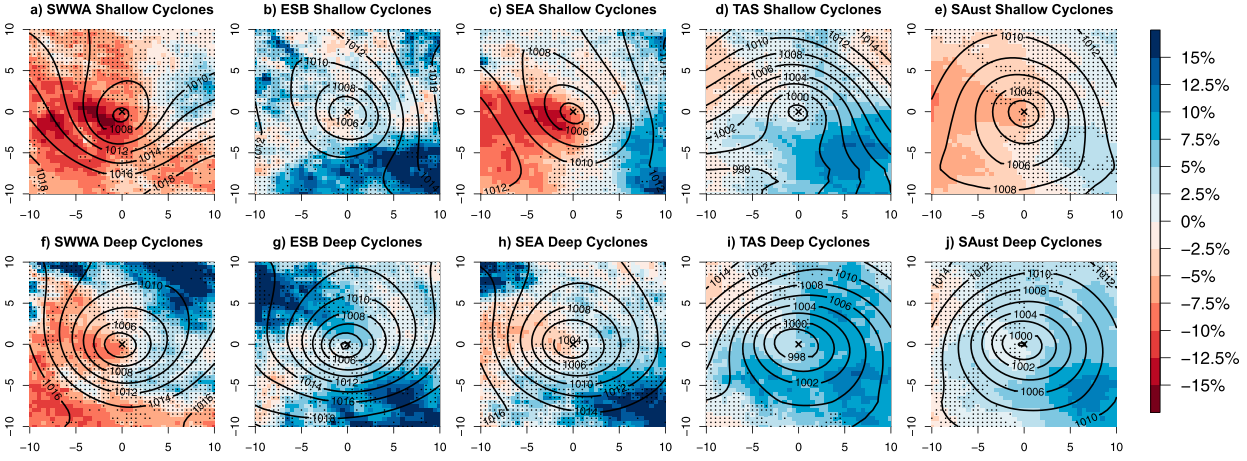

FIG. 11. Composite mean sea level pressure (black contours; every 2 hPa) for all RCM cyclones in 1980–2009, and the ensemble mean change in rain rate between 1980–2009 and 2070–99 (shaded; % K^{-1}), for (a)–(e) shallow surface cyclones and (f)–(j) deep cyclones. Columns show cyclones in five different subregions, with all southern Australian cyclones in (e) and (j). Stippling indicates where fewer than 10 models agree on the sign of the change.

Unauthenticated | Downloaded 06/19/24 09:21 PM UTC

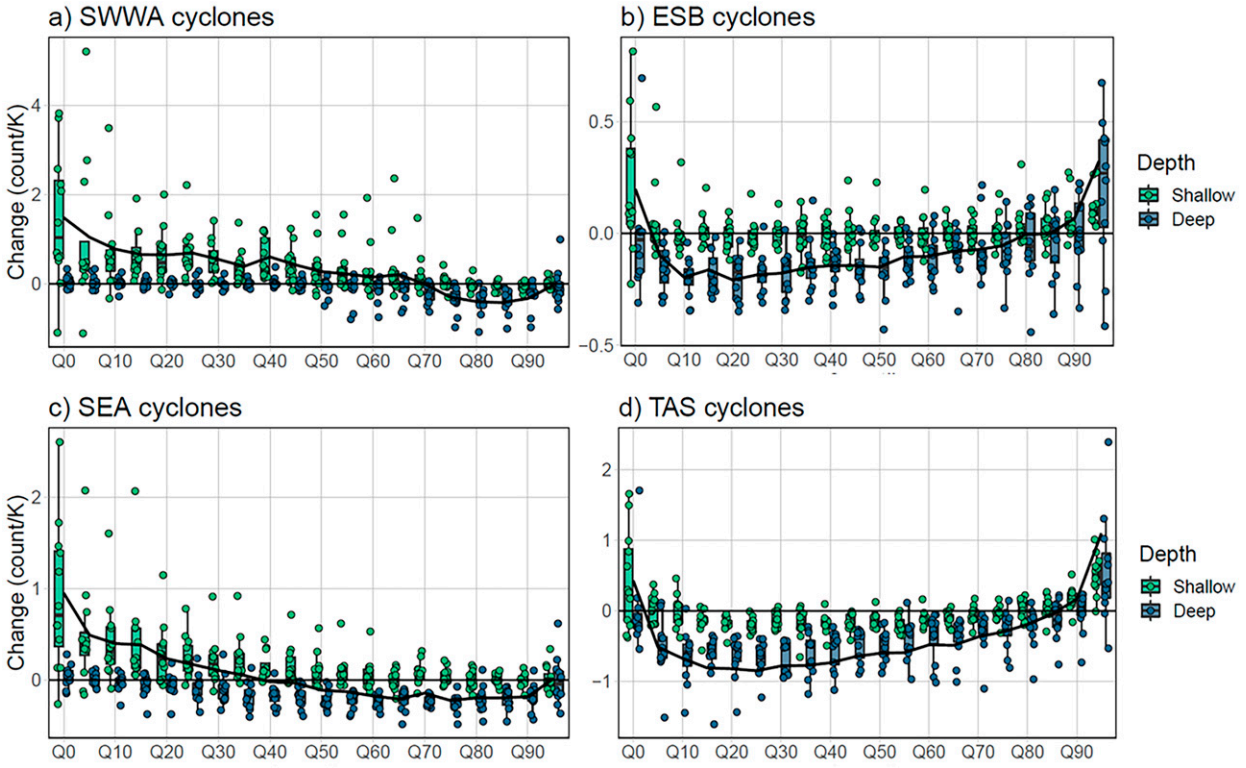

FIG. 12. Change in annual frequency of surface cyclones with different mean rain rates within 5° of the cyclone center for each region between 1980–2009 and 2070–99 (counts per kelvin). Data are normalized to the historical quantiles of cyclone mean rain rate for each model so that the first box shows changes in the number of cyclones with rain rates in the bottom 5% of current cyclones for that model, etc. Each dot gives the change for a single RCM, with colors indicating shallow (green) and deep (blue) cyclones; the black line indicates the ensemble mean change in the total number of cyclones exceeding each intensity threshold. The *x* axes give the quantiles, with Q10 referring to the 10th percentile, etc.

heavy localized rain as in 1980–2009 (Fig. S9 in the online supplemental material). More than 90% of model simulations have at least one cyclone in 2070–99 that has a higher maximum rain rate than any observed in 1980–2009 in both SEA and Tasmania, as well as 75% of models in the ESB.

In contrast to projected increases in cyclones with heavy rain rates, there are no notable changes projected in the frequency of cyclones with maximum wind speeds exceeding the 95th percentile in either Tasmania or the ESB (Fig. S10 in the online supplemental material). Consistent with the projected decrease in mean cyclone intensity, cyclones with strong winds are projected to become less common in the future in both SEA ($-5.9\%\ K^{-1}$) and SWWA ($-6.8\%\ K^{-1}$). However, this is based on hourly wind data, and results could differ for shorter-duration wind extremes.

6. Discussion

GCMs can broadly replicate the general features of the global cyclone climatology at both surface and upper levels. However, biases remain in GCM cyclone simulations, including a tendency to overestimate the frequency of surface cyclones over land during the warm months and underestimate the frequency of cyclones south of Australia (Dowdy et al. 2013; Pepler and Dowdy 2021a; Priestley et al. 2020). All three downscaling methods used in this paper show a marked improvement in simulated cyclone frequency relative to the driving GCMs, consistent with previous studies using RegCM4 for the Southern Hemisphere midlatitudes (Reboita et al. 2021). This improvement is likely a result of the finer spatial resolution of the RCMs, which allows them to better simulate small-scale features important to cyclone development including the role of heavy rainfall and diabatic heating (McInnes et al. 1992), as well as how cyclones interact with coastal topography (Pepler et al. 2017), which is poorly represented in coarser GCMs. The RCMs are also well able to simulate the mean MSLP and rain patterns around cyclones in different parts of Australia, including their contribution to total Australian rainfall and extremes, although the contribution of cyclones to rainfall near the borders of the RCM domain is likely to be underestimated.

GCMs consistently project an expansion of the tropics and a corresponding poleward shift in the Southern Hemisphere midlatitude storm track (IPCC 2021). Consistent with this global trend as well as previous GCM-based studies (Dowdy et al. 2014; Pepler and Dowdy 2021a), the 12 RCMs used in this study project a robust decline in the frequency of deep cyclones over southern Australia during the twenty-first

Unauthenticated | Downloaded 06/19/24 09:21 PM UTC

century, by about 11% for each additional degree of mean global surface temperature. The associated decline in rainfall from deep cyclones (-10% K^{-1}) explains more than 80% of the projected decline in total cool-season rainfall in southern Australia. By separating the cyclone and noncyclone components of rainfall we show that the intermodel uncertainty in future rainfall projection is dominated by uncertainty in projections of noncyclone rainfall including thunderstorms and fronts, which are the other major causes of rainfall in southern Australia (Dowdy 2020b; Pepler et al. 2020). Although further constraining projected convective rainfall remains a challenge, because convection is parameterized at the scale of RCMs in this paper, understanding the robust forced signal in cyclone-related rainfall may assist in planning, particularly for applications where large-scale extreme rainfall such as produced by cyclones is particularly important such as water security (Pepler and Rakich 2010) or large-scale riverine flooding (Power and Callaghan 2016).

In contrast to deep cyclones, the frequency of shallow surface cyclones is projected to increase, particularly during the summer months. Such cyclones are typically weaker in intensity and shorter in duration, so have not necessarily been identified in studies that focus on projections of long-lived extratropical cyclones and/or the cool season only (Priestley and Catto 2022; Grieger et al. 2014). In many cases these are likely to be heat lows (Lavender 2017), particularly in the mainly inland areas of SEA and SWWA, where average rain rates for shallow cyclones are low and the projected increase is dominated by an increase in cyclones with lower rain rates and wind speeds. An increase in heat lows is likely a response to the enhanced warming projected for land areas compared during the twenty-first century (IPCC 2021), as heat lows are an atmospheric response to surface heating. However, some shallow surface cyclones can produce very heavy rain, particularly on the east coast of Australia and near Tasmania, where shallow surface lows and hybrid lows can produce significant impacts and should not be neglected in projections (Cavicchia et al. 2020; Pepler and Dowdy 2021b). The projected increase in shallow surface cyclones with heavy rain in these regions is likely associated with the very strong warming projected for the East Australian Current, as shallow surface cyclones are more frequent when SSTs are elevated (Pepler et al. 2016b) and their location including associated convection and rainfall can be influenced by SST eddies (Chambers et al. 2014). This could also be linked to increases in moisture availability and rain rates, as diabatic forcing can play an important role in cyclone development in southeast Australia (McInnes et al. 1992).

The average intensity of cyclones as measured by the Laplacian of MSLP or the average 1-h winds is projected to decrease, particularly in SEA and SWWA where weak heat lows form an increasing proportion of cyclones, in contrast to projections of intensified Southern Hemisphere cyclones more generally (Priestley and Catto 2022). However, no change is projected in the average Laplacian of deep cyclones, which are expected to decrease in frequency across the whole intensity distribution. There is no change or a decrease projected in the frequency of cyclones with very strong winds, defined as exceeding the present-day 95th percentile of maximum winds, although projections may differ for extreme winds on shorter time scales, which may be less well simulated in current RCMs (Brown and Dowdy 2021).

The average maximum rain intensity for both deep and shallow cyclones is projected to increase in both the ESB and Tasmania by close to the Clausius–Clapeyron relationship of 7% K^{-1}. This is consistent with global increases in the moisture available for heavy rainfall in a warmer world (Pfahl et al. 2017; O'Gorman and Muller 2010), as well as projected increases in moisture flux into southeast Australia during extreme atmospheric rivers, which can contribute to heavy rainfall during cyclones (Reid et al. 2021). This reflects a fundamental shift in the distribution of cyclone rainfall, with a decrease projected in the frequency of cyclones with moderate rainfall but an increase in the frequency of the most intense cyclones with rain rates exceeding the current 95th percentile. Consequently, most regions of southern Australia project a decrease in total annual rainfall from deep cyclones, but no change or an increase in cyclone-related days with rainfall exceeding the current annual maximum of daily rainfall ("Rx1D"). More than 75% of models also simulate cyclones in 2070–99 with peak rain rates in SEA, Tasmania, and the ESB that exceed any event in the 1980–2009 period, suggesting a potential for record-breaking extreme rainfall in future cyclones. However, it is important to note that this short period may not fully capture the large range of historical cyclone extremes (Callaghan and Power 2014). An increase in cyclone rainfall intensity is consistent with previous studies using older RCM approaches (Cavicchia et al. 2020; Pepler et al. 2016a; Reboita et al. 2021).

In addition to considering these RCM projections of cyclone-related rainfall, the remaining rainfall can also be considered (i.e., noncyclone rainfall). As compared with cyclone-related rainfall, future projections of noncyclone rainfall remain uncertain for large areas of Australia. However, we identify three regions of strong intermodel agreement as areas for future work:

1) A projected decline in noncyclone rainfall in southwest WA rainfall during the cool season. This is related to declines in frontal rainfall (Hope et al. 2006), although Utsumi et al. (2016) also found that cyclones and fronts together did not explain all of the projected decline in this region.
2) A projected decline in noncyclone rainfall in parts of northeast Australia during the cool season. While this is the drier season in this region, a decline has also been observed here in recent decades (Dey et al. 2019).
3) A projected increase in noncyclone rainfall on the east coast, particularly in the warm season, including an increase in noncyclone extreme rainfall. This could be related to changes in some factors such as convective precipitation from thunderstorms (Dowdy 2020a), high pressure systems, and onshore easterly winds, which are important for rainfall in this region (Black and Lane 2015; Callaghan and Power 2016; Pepler et al. 2020), changes in moisture flux such as atmospheric rivers (Reid et al. 2021)

Unauthenticated | Downloaded 06/19/24 09:21 PM UTC

and shifts in the location of the subtropical ridge (Timbal and Drosdowsky 2013).

This paper has taken advantage of the finer resolution of RCMs to provide detailed projections of cyclone-related rainfall, with the current generation of RCMs able to simulate key aspects of observed cyclone climatology in Australia. There is now a robust consensus that cyclone-related total rainfall is likely to decline over southern mainland Australia, explaining the majority of projected cool-season rainfall declines, while in some contrast cyclone-related heavy rainfall remains nearly constant or increases. However, the RCMs continue to slightly underestimate the frequency of deep cyclones and their importance to rainfall in the current climate, such that a similar percentage change in cyclones to that projected could potentially result in even larger future declines in cool-season rainfall than the models indicate. The decrease in cyclone-related strong winds and increase in intense rainfall, combined with an underlying increase in sea level (Hague et al. 2020, 2022), suggests an increase in the relative contribution of flooding to total damages from extratropical cyclones.

This might be further improved on using downscaled CMIP6 data, as CMIP6 has been shown to incrementally improve the representation of Southern Hemisphere cyclones, particularly for high-resolution GCMs (Priestley et al. 2020). Potential next steps could also consider building on this study's methods but applied to finer-scale RCMs than those used here (e.g., convection-permitting simulations), as thunderstorms can play an important role in cyclone-associated rainfall, particularly on the east coast (Dowdy and Catto 2017). However, the largest uncertainty in future projections is in noncyclone rainfall, which may potentially only be resolved by improvements in approaches for simulating fine-scale physical processes around convective storms, as might potentially become more feasible in future RCMs at convection-permitting scales.

Acknowledgments. This study was supported through the Australian Government's Climate Systems hub of the National Environmental Science Program (NESP). We thank Irina Rudeva and Dörte Jakob for their helpful comments on this paper, as well as three anonymous reviewers whose detailed comments significantly improved it. We also thank all the modeling groups whose data contributed to this paper, including those that contributed to CMIP5; the NARCliM1.5 modeling team including Jason Evans, Giovanni di Virgilio, Nidhi Nishant, and Fei Ji; the CCAM modeling team at CSIRO including Marcus Thatcher; and others in the BARPA modeling team at the Bureau of Meteorology including Chun-Hsu Su, Harvey Ye, Christian Stassen, Peter Steinle, and Greg Roff.

Data availability statement. All regional model data remain the property of the generating group—BARPA is generated by the Bureau of Meteorology, CCAM is generated by CSIRO, and NARCliM1.5 is generated by UNSW and the NSW DPE. Cyclone track data from ERA5 and CMIP5 are available online (https://doi.org/10.6084/m9.figshare.13393172.v1), and RCM cyclone tracks generated for this paper are also available (https://doi.org/10.6084/m9.figshare.19669518.v1). For access to larger derived grids such as cyclone-centered composite data, contact the author (acacia.pepler@bom.gov.au).

REFERENCES

Black, M. T., and T. P. Lane, 2015: An improved diagnostic for summertime rainfall along the eastern seaboard of Australia. *Int. J. Climatol.*, **35**, 4480–4492, https://doi.org/10.1002/joc.4300.

BoM and CSIRO, 2020: State of the Climate 2020. CSIRO and Bureau of Meteorology, 24 pp., https://www.csiro.au/en/research/environmental-impacts/climate-change/state-of-the-climate.

Booth, J. F., C. M. Naud, and J. Jeyaratnam, 2018: Extratropical cyclone precipitation life cycles: A satellite-based analysis. *Geophys. Res. Lett.*, **45**, 8647–8654, https://doi.org/10.1029/2018GL078977.

Brown, A., and A. Dowdy, 2021: Severe convective wind environments and future projected changes in Australia. *J. Geophys. Res. Atmos.*, **126**, e2021JD034633, https://doi.org/10.1029/2021JD034633.

Callaghan, J., and S. Power, 2014: Major coastal flooding in southeastern Australia, associated deaths and weather systems. *Aust. Meteor. Oceanogr. J.*, **64**, 183–213, https://doi.org/10.22499/2.6403.002.

——, and ——, 2016: A vertical wind structure that leads to extreme rainfall and major flooding in southeast Australia. *J. South. Hemisphere Earth Syst. Sci.*, **66**, 380–401, https://doi.org/10.22499/3.6604.002.

Cavicchia, L., A. Pepler, A. Dowdy, J. Evans, A. Di Luca, and K. Walsh, 2020: Future changes in the occurrence of hybrid cyclones: The added value of cyclone classification for the East Australian low-pressure systems. *Geophys. Res. Lett.*, **47**, e2019GL085751, https://doi.org/10.1029/2019GL085751.

Chambers, C. R. S., G. B. Brassington, I. Simmonds, and K. Walsh, 2014: Precipitation changes due to the introduction of eddy-resolved sea surface temperatures into simulations of the "Pasha Bulker" Australian east coast low of June 2007. *Meteor. Atmos. Phys.*, **125** (1–2), 1–15, https://doi.org/10.1007/s00703-014-0318-4.

CSIRO and BoM, 2015: Climate change in Australia projections for Australia's natural resource management regions. CSIRO and Bureau of Meteorology Tech. Rep., 222 pp., https://www.climatechangeinaustralia.gov.au/media/ccia/2.2/cms_page_media/168/CCIA_2015_NRM_TechnicalReport_WEB.pdf.

Dey, R., S. C. Lewis, J. M. Arblaster, and N. J. Abram, 2019: A review of past and projected changes in Australia's rainfall. *Wiley Interdiscip. Rev.: Climate Change*, **10**, e577, https://doi.org/10.1002/wcc.577.

Di Luca, A., J. P. Evans, A. Pepler, L. Alexander, and D. Argüeso, 2014: Resolution sensitivity of cyclone climatology over eastern Australia using six reanalysis products. *J. Climate*, **28**, 9530–9549, https://doi.org/10.1175/JCLI-D-14-00645.1.

——, ——, ——, ——, and ——, 2016: Evaluating the representation of Australian East Coast lows in a regional climate model ensemble. *J. South. Hemisphere Earth Syst. Sci.*, **66**, 108–124, https://doi.org/10.1071/ES16011.

Di Virgilio, G., J. P. Evans, A. Di Luca, M. R. Grose, V. Round, and M. Thatcher, 2020: Realised added value in dynamical downscaling of Australian climate change. *Climate Dyn.*, **54**, 4675–4692, https://doi.org/10.1007/s00382-020-05250-1.

Unauthenticated | Downloaded 06/19/24 09:21 PM UTC

Dowdy, A. J., 2020a: Seamless climate change projections and seasonal predictions for bushfires in Australia. *J. South. Hemisphere Earth Syst. Sci.*, **70**, 120–138, https://doi.org/10.1071/ES20001.

——, 2020b: Climatology of thunderstorms, convective rainfall and dry lightning environments in Australia. *Climate Dyn.*, **54**, 3041–3052, https://doi.org/10.1007/s00382-020-05167-9.

——, and J. L. Catto, 2017: Extreme weather caused by concurrent cyclone, front and thunderstorm occurrences. *Sci. Rep.*, **7**, 40359, https://doi.org/10.1038/srep40359.

——, G. A. Mills, B. Timbal, and Y. Wang, 2013: Changes in the risk of extratropical cyclones in eastern Australia. *J. Climate*, **26**, 1403–1417, https://doi.org/10.1175/JCLI-D-12-00192.1.

——, ——, ——, and ——, 2014: Fewer large waves projected for eastern Australia due to decreasing storminess. *Nat. Climate Change*, **4**, 283–286, https://doi.org/10.1038/nclimate2142.

——, and Coauthors, 2021: Extreme temperature, wind and bushfire weather projections using a standardised method. Bureau of Meteorology Bureau Research Rep. BRR055, 63 pp.

Evans, J. P., G. Di Virgilio, A. L. Hirsch, P. Hoffmann, A. R. Remedio, F. Ji, B. Rockel, and E. Coppola, 2021: The CORDEX-Australasia ensemble: Evaluation and future projections. *Climate Dyn.*, **57**, 1385–1401, https://doi.org/10.1007/s00382-020-05459-0.

Fandry, C. B., and L. M. Leslie, 1984: A two-layer quasi-geostrophic model of summer trough formation in the Australian subtropical easterlies. *J. Atmos. Sci.*, **41**, 807–818, https://doi.org/10.1175/1520-0469(1984)041<0807:ATLQGM>2.0.CO;2.

Fiddes, S., A. Pepler, K. Saunders, and P. Hope, 2021: Redefining southern Australia's climatic regions and seasons. *J. South. Hemisphere Earth Syst. Sci.*, **71**, 92–109, https://doi.org/10.1071/ES20003.

Grieger, J., G. C. Leckebusch, M. G. Donat, M. Schuster, and U. Ulbrich, 2014: Southern Hemisphere winter cyclone activity under recent and future climate conditions in multi-model AOGCM simulations. *Int. J. Climatol.*, **34**, 3400–3416, https://doi.org/10.1002/joc.3917.

Hague, B. S., S. McGregor, B. F. Murphy, R. Reef, and D. A. Jones, 2020: Sea-level rise driving increasingly predictable coastal inundation in Sydney, Australia. *Earth's Future*, **8**, e2020EF001607, https://doi.org/10.1029/2020EF001607.

——, D. A. Jones, D. Jakob, S. McGregor, and R. Reef, 2022: Australian coastal flooding trends and forcing factors. *Earth's Future*, **10**, e2021EF002483, https://doi.org/10.1029/2021EF002483.

Hawcroft, M. K., L. C. Shaffrey, K. I. Hodges, and H. F. Dacre, 2012: How much Northern Hemisphere precipitation is associated with extratropical cyclones? *Geophys. Res. Lett.*, **39**, L24809, https://doi.org/10.1029/2012GL053866.

Hersbach, H., and Coauthors, 2020: The ERA5 global reanalysis. *Quart. J. Roy. Meteor. Soc.*, **146**, 1999–2049, https://doi.org/10.1002/qj.3803.

Hope, P. K., W. Drosdowsky, and N. Nicholls, 2006: Shifts in the synoptic systems influencing southwest Western Australia. *Climate Dyn.*, **26**, 751–764, https://doi.org/10.1007/s00382-006-0115-y.

Hopkins, L. C., and G. J. Holland, 1997: Australian heavy-rain days and associated East Coast cyclones: 1958–92. *J. Climate*, **10**, 621–635, https://doi.org/10.1175/1520-0442(1997)010<0621:AHRDAA>2.0.CO;2.

IPCC, 2021: *Climate Change 2021: The Physical Science Basis*. Cambridge University Press, 3949 pp., https://www.ipcc.ch/report/ar6/wg1/.

Jones, D. A., W. Wang, and R. Fawcett, 2009: High-quality spatial climate data-sets for Australia. *Aust. Meteor. Oceanogr. J.*, **58**, 233–248, https://doi.org/10.22499/2.5804.003.

Kobayashi, S., and Coauthors, 2015: The JRA-55 reanalysis: General specifications and basic characteristics. *J. Meteor. Soc. Japan*, **93**, 5–48, https://doi.org/10.2151/jmsj.2015-001.

Lavender, S. L., 2017: A climatology of Australian heat low events. *Int. J. Climatol.*, **37**, 534–539, https://doi.org/10.1002/joc.4692.

McInnes, K. L., L. M. Leslie, and J. L. McBride, 1992: Numerical simulation of cut-off lows on the Australian east coast: Sensitivity to sea-surface temperature. *Int. J. Climatol.*, **12**, 783–795, https://doi.org/10.1002/joc.3370120803.

Murray, R. J., and I. Simmonds, 1991: A numerical scheme for tracking cyclone centres from digital data. Part I: Development and operation of the scheme. *Aust. Meteor. Mag.*, **39**, 155–166, http://www.bom.gov.au/jshess/papers.php?year=1991.

Neu, U., and Coauthors, 2013: IMILAST: A community effort to intercompare extratropical cyclone detection and tracking algorithms. *Bull. Amer. Meteor. Soc.*, **94**, 529–547, https://doi.org/10.1175/BAMS-D-11-00154.1.

O'Gorman, P. A., and C. J. Muller, 2010: How closely do changes in surface and column water vapor follow Clausius-Clapeyron scaling in climate change simulations? *Environ. Res. Lett.*, **5**, 025207, https://doi.org/10.1088/1748-9326/5/2/025207.

Pendergrass, A. G., F. Lehner, B. M. Sanderson, and Y. Xu, 2015: Does extreme precipitation intensity depend on the emissions scenario? *Geophys. Res. Lett.*, **42**, 8767–8774, https://doi.org/10.1002/2015GL065854.

Pepler, A. S., and C. S. Rakich, 2010: Extreme inflow events and synoptic forcing in Sydney catchments. *IOP Conf. Ser. Earth Environ. Sci.*, **11**, 012010, https://doi.org/10.1088/1755-1315/11/1/012010.

——, and A. Dowdy, 2020: A three-dimensional perspective on extratropical cyclone impacts. *J. Climate*, **33**, 5635–5649, https://doi.org/10.1175/JCLI-D-19-0445.1.

——, and ——, 2021a: Fewer deep cyclones projected for the midlatitudes in a warming climate, but with more intense rainfall. *Environ. Res. Lett.*, **16**, 054044, https://doi.org/10.1088/1748-9326/abf528.

——, and ——, 2021b: Intense east coast lows and associated rainfall in eastern Australia. *J. South. Hemisphere Earth Syst. Sci.*, **71**, 110–122, https://doi.org/10.1071/ES20013.

——, A. Di Luca, F. Ji, L. V. Alexander, J. P. Evans, and S. C. Sherwood, 2015: Impact of identification method on the inferred characteristics and variability of Australian East Coast lows. *Mon. Wea. Rev.*, **143**, 864–877, https://doi.org/10.1175/MWR-D-14-00188.1.

——, ——, ——, ——, ——, and ——, 2016a: Projected changes in East Australian midlatitude cyclones during the 21st century. *Geophys. Res. Lett.*, **43**, 334–340, https://doi.org/10.1002/2015GL067267.

——, L. V. Alexander, J. P. Evans, and S. C. Sherwood, 2016b: The influence of local sea surface temperatures on Australian east coast cyclones. *J. Geophys. Res. Atmos.*, **121**, 13 352–13 363, https://doi.org/10.1002/2016JD025495.

——, ——, ——, and ——, 2017: The influence of topography on midlatitude cyclones on Australia's east coast. *J. Geophys. Res. Atmos.*, **122**, 9173–9184, https://doi.org/10.1002/2017JD027345.

——, P. Hope, and A. Dowdy, 2019: Long-term changes in southern Australian anticyclones and their impacts. *Climate Dyn.*, **53**, 4701–4714, https://doi.org/10.1007/s00382-019-04819-9.

Unauthenticated | Downloaded 06/19/24 09:21 PM UTC

——, A. J. Dowdy, P. van Rensch, I. Rudeva, J. L. Catto, and P. Hope, 2020: The contributions of fronts, lows and thunderstorms to southern Australian rainfall. *Climate Dyn.*, **55**, 1489–1505, https://doi.org/10.1007/s00382-020-05338-8.

——, ——, and P. Hope, 2021: The differing role of weather systems in southern Australian rainfall between 1979–1996 and 1997–2015. *Climate Dyn.*, **56**, 2289–2302, https://doi.org/10.1007/s00382-020-05588-6.

Pfahl, S., and H. Wernli, 2012: Quantifying the relevance of cyclones for precipitation extremes. *J. Climate*, **25**, 6770–6780, https://doi.org/10.1175/JCLI-D-11-00705.1.

——, P. A. O'Gorman, and E. M. Fischer, 2017: Understanding the regional pattern of projected future changes in extreme precipitation. *Nat. Climate Change*, **7**, 423–427, https://doi.org/10.1038/nclimate3287.

Power, S. B., and J. Callaghan, 2016: Variability in severe coastal flooding, associated storms, and death tolls in southeastern Australia since the mid-nineteenth century. *J. Appl. Meteor. Climatol.*, **55**, 1139–1149, https://doi.org/10.1175/JAMC-D-15-0146.1.

Priestley, M. D. K., and J. L. Catto, 2022: Future changes in the extratropical storm tracks and cyclone intensity, wind speed, and structure. *Wea. Climate Dyn.*, **3**, 337–360, https://doi.org/10.5194/wcd-3-337-2022.

——, D. Ackerley, J. L. Catto, K. I. Hodges, R. E. McDonald, and R. W. Lee, 2020: An overview of the extratropical storm tracks in CMIP6 historical simulations. *J. Climate*, **33**, 6315–6343, https://doi.org/10.1175/JCLI-D-19-0928.1.

Reboita, M. S., and Coauthors, 2021: Future changes in the wintertime cyclonic activity over the CORDEX-CORE Southern Hemisphere domains in a multi-model approach. *Climate Dyn.*, **57**, 1533–1549, https://doi.org/10.1007/s00382-020-05317-z.

Reid, K. J., T. A. O'Brien, A. D. King, and T. P. Lane, 2021: Extreme water vapor transport during the March 2021 Sydney floods in the context of climate projections. *Geophys. Res. Lett.*, **48**, e2021GL095335, https://doi.org/10.1029/2021GL095335.

Risbey, J. S., P. C. McIntosh, and M. J. Pook, 2013: Synoptic components of rainfall variability and trends in southeast Australia. *Int. J. Climatol.*, **33**, 2459–2472, https://doi.org/10.1002/joc.3597.

Schwalm, C. R., S. Glendon, and P. B. Duffy, 2020: RCP8.5 tracks cumulative CO_2 emissions. *Proc. Natl. Acad. Sci. USA*, **117**, 19 656–19 657, https://doi.org/10.1073/pnas.2007117117.

Simmonds, I., R. J. Murray, and R. M. Leighton, 1999: A refinement of cyclone tracking methods with data from FROST. *Aust. Meteor. Mag.*, Special Issue, 35–49, http://www.bom.gov.au/jshess/papers.php?year=1999.

Su, C.-H., and Coauthors, 2019: BARRA v1.0: The Bureau of Meteorology Atmospheric High-Resolution Regional Reanalysis for Australia. *Geosci. Model Dev.*, **12**, 2049–2068, https://doi.org/10.5194/gmd-12-2049-2019.

——, H. Ye, A. Dowdy, A. Pepler, C. Stassen, A. Brown, S. O. Tucker, and P. J. Steinle, 2021: Towards ACCESS-based regional climate projections for Australia. Bureau of Meteorology Bureau Research Rep. BRR057, 41 pp.

Taylor, K. E., R. J. Stouffer, and G. A. Meehl, 2012: An overview of CMIP5 and the experiment design. *Bull. Amer. Meteor. Soc.*, **93**, 485–498, https://doi.org/10.1175/BAMS-D-11-00094.1.

Thatcher, M., and J. L. McGregor, 2011: A technique for dynamically downscaling daily-averaged GCM datasets using the conformal cubic atmospheric model. *Mon. Wea. Rev.*, **139**, 79–95, https://doi.org/10.1175/2010MWR3351.1.

Timbal, B., and W. Drosdowsky, 2013: The relationship between the decline of southeastern Australian rainfall and the strengthening of the subtropical ridge. *Int. J. Climatol.*, **33**, 1021–1034, https://doi.org/10.1002/joc.3492.

Utsumi, N., H. Kim, S. Kanae, and T. Oki, 2016: Which weather systems are projected to cause future changes in mean and extreme precipitation in CMIP5 simulations? *J. Geophys. Res. Atmos.*, **121**, 10 522–10 537, https://doi.org/10.1002/2016JD024939.

——, ——, ——, and ——, 2017: Relative contributions of weather systems to mean and extreme global precipitation. *J. Geophys. Res. Atmos.*, **122**, 152–167, https://doi.org/10.1002/2016JD025222.

Unauthenticated | Downloaded 06/19/24 09:21 PM UTC